Vacuum 108 (2014) 66–70

Contents lists available at ScienceDirect

Vacuum

journal homepage: www.elsevier.com/locate/vacuum

Rapid communication

High temperature oxidation of Cr–N coatings prepared by high power pulsed magnetron sputtering – Plasma immersion ion implantation & deposition

Zhongzhen Wu [a, b], Xiubo Tian [b, **], Shu Xiao [a], Chunzhi Gong [b], Feng Pan [a, *], Paul K. Chu [c]

[a] School of Advanced Materials, Peking University Shenzhen Graduate School, Shenzhen 518055, China
[b] State Key Laboratory of Advanced Welding Production and Technology, Harbin Institute of Technology, Harbin 150001, China
[c] Department of Physics and Materials Science, City University of Hong Kong, Tat Chee Avenue, Kowloon, Hong Kong, China

ARTICLE INFO

Article history:
Received 29 April 2014
Received in revised form
11 May 2014
Accepted 2 June 2014
Available online 14 June 2014

Keywords:
HPPMS-PIII&D
Cr–N
High temperature oxidation
Corrosion resistance

ABSTRACT

Good oxidation and corrosion resistance are required for cutting tools and other industrial components used in high temperature applications. The highest operational temperature of CrN is normally about 500 °C. A denser Cr–N coating prepared by high power pulsed magnetron sputtering – plasma immersion ion implantation & deposition shows oxidation resistance up to 800 °C compare with those prepared by conventional magnetron sputtering. The hardness and corrosion resistance are shown and discussed. The enhanced performance can be attributed to a phase transition from CrN to Cr_2N during annealing and there is no obvious oxide formation on the coatings.

Good thermal oxidation resistance and corrosion resistance are needed for high-speed cutting tools and industrial components used in harsh environments, for instance, pipelines, boilers, etc. [1–3] and a feasible method to protect the components from high temperature oxidation and corrosion is to apply a surface coatings. However, there are normally oxidation and corrosion channels in coatings prepared by conventional PVD methods such as cathodic arc deposition and magnetron sputtering because cavities induced by the "macro-particles" and low energetic deposition, respectively [4,5].

High power pulsed magnetron sputtering – plasma immersion ion implantation & deposition (HPPMS-PIII&D) is a relatively new hybrid technology [6,7] combining high plasma ionization of high power pulsed magnetron sputtering (HPPMS) and consequent high energetic ion acceleration of plasma immersion ion implantation & deposition (PIII&D). By combining the high ionization efficiency in HPPMS and energetic ion bombardment and implantation rendered by PIII&D, an extra dense coatings with better oxidation and corrosion resistance can be prepared [8,9]. CrN is commonly applied as a coating due to its excellent oxidation and corrosion resistance but CrN coatings prepared by conventional PVD methods resist oxidation and degradation of mechanical properties only up to about 500 °C [10,11] which is insufficient in many demanding applications.

In this work, Cr–N coatings are prepared by HPPMS-PIII&D and the oxidation and corrosion resistance of the Cr–N coatings is studied after annealing at different temperatures. The performance of these coatings is compared to that produced by conventional direct-current magnetron sputtering (DCMS) and high power pulsed magnetron sputtering (HPPMS) with −100 V DC bias. The Cr–N coatings prepared by the HPPMS-PIII&D deliver outstanding protection even after the annealing at a temperature as high as 800 °C.

Deposition was performed in a vacuum chamber (40 cm in diameter and 80 cm in height) evacuated by a turbo-molecular pump and it was carried out in three stages. Firstly, a Cr layer was produced on Si (100) (for SEM and TEM observation) and SU201 stainless steel (for other tests) substrates by HPPMS-PIII&D at 780 V, 50 Hz and 200 μs in an inert atmosphere. The high-voltage pulses applied to the substrates had amplitudes of −8 kV, −12 kV, −16 kV, and −20 kV and the same frequency and width as those of the HPPMS pulses. The high voltage and HPPMS

* Corresponding author. Tel./fax: +86 755 26033200.
** Corresponding author. Tel./fax: +86 451 86418784.
E-mail addresses: wuzhongzhen2003@163.com (Z. Wu), xiubotian@163.com (X. Tian), panfeng@pkusz.edu.cn (F. Pan).

http://dx.doi.org/10.1016/j.vacuum.2014.06.002
0042-207X/

pulses were synchronized by a matching circuit [6]. The working pressure was kept 1.0 Pa for 5 min. The substrates were placed at a distance of 16 cm from the target and not treated during deposition. In the second stage, N_2 was introduced into the vacuum chamber gradually until the flow rate ratio of Ar to N_2 was 5:3. Cr–N thin films with a thickness of 1.5 μm were deposited in this mixed atmosphere. Finally, cool down in the vacuum chamber for 30 min. For comparison, conventional DCMS and HPPMS were conducted to deposit Cr–N at a DC bias of −100 V and the same power as that in HPPMS-PIII&D. The thickness and Cr/N ratio of the materials prepared by DCMS and HPPMS are similar to those prepared by HPPMS-PIII&D at −12 kV, which is about 1:1.

After deposition, the samples were annealed in an oven for 1 h at 200 °C, 400 °C, 600 °C, or 800 °C. The microstructure and thickness of the coatings were evaluated by scanning electron microscopy (SEM) on a 30 kV Hitachi S4800 instrument. The cross sections and interfaces were examined by high-resolution transmission electron microscopy (FE-TEM, FEI-TECNAIG2-F30, USA). X-ray diffraction (XRD) was performed to investigate the phase composition of the films using the Bragg–Brentano geometry. A Cu K_α radiation source was used (40 kV, 40 mA). An MTS nano-indenter XPII equipped with a Berkovich diamond indenter was used to measure the hardness and Young's modulus of the samples and the corrosion behaviors of the samples were studied by electrochemical methods. A computer-assisted electrochemical apparatus was used to obtain the potential–current curves. The polarization plots were acquired in a 3.5% NaCl solution at a scanning rate of 5 mV/s.

Fig. 1 depicts the SEM cross-sectional micrographs of the Cr–N films fabricated by DCMS and HPPMS with DC bias of −100 V and HPPMS-PIII&D with pulsed bias of −12 kV. The DCMS sample exhibits a loosely packed columnar structure (Fig. 1a) and most of columnar grains are continuous from the substrate to the coating surface. A columnar structure typically forms during low-energy deposition due to low adatom mobility [12]. A well-defined boundary and abrupt interface appear between the substrate and Cr–N film indicative of potentially bad film adhesion. The HPPMS sample shows a dense granular nano-crystalline structure and clean interface are observed [13]. In comparison, the HPPMS-PIII&D sample shows a most densely packed columnar structure (Fig. 1b) and most of the columns are discontinuous. The top columns seem to form on the broken columns quickly due to re-nucleation [14]. An extra dense structure without any cavities can be observed between the Cr–N columnar crystals (Fig. 1c). The interface provides a direct contact between the dense granular nano-crystalline Cr interlayer and substrate thus promoting the formation of metallic, covalent, or ionic bonds as opposed to the significantly weaker van der Waals bonds (Fig. 1d). Formation of the dense coating and compact interface arises from the relatively high energy of about 12 keV and consequent thermal diffusion [15].

Fig. 2 displays the XRD spectra acquired from the as-prepared Cr–N films fabricated by DCMS and HPPMS at a DC bias of −100 V and HPPMS-PIII&D at pulsed biases of −8 kV, −12 kV, −16 kV, and −20 kV. For the DCMS and HPPMS samples, the CrN(200), Cr_2N(113) peak and some peaks stemming from the substrate can be observed. The intensity of the peaks is low and some peaks are broad suggesting the existence of amorphous or nano-crystals in the films. A large difference can be observed from the HPPMS-PIII&D samples which show a highly preferential orientation of CrN(200) and some weaker peaks introduced by the stainless steel substrate. With increasing pulsed biases, the intensity of the CrN(200) peak decreases and the Cr_2N(111) peak appears when the pulsed bias is larger than −16 kV. The phase evolution may depend on the N contents in the Cr–N coatings which decrease because more Cr ions are attracted to the substrate while the Ar/N ratio in the ambient is kept constant.

Fig. 3 shows the XRD spectra of the Cr–N films fabricated by DCMS and HPPMS at −100 V and HPPMS-PIII&D at −12 kV after annealing at different temperature from room temperature to 800 °C. When the annealing temperature is below 600 °C, there are nearly no peak changes in all the Cr–N coatings. prepared by DCMS and HPPMS. However, many new peaks such as CrN(110), Cr_2N(302), Cr_2N(111), Cr_2N(221), Cr_2O_3(104), Cr_2O_3(300), and Cr_2O_3(210) emerge on the Cr–N coatings prepared by DCMS and HPPMS after annealing at 600 °C and they increase further after annealing at 800 °C (Fig. 3a). The peak intensity of the DCMS sample increases with annealing temperature, indicating continuous oxidation and also re-crystallization [16]. The oxidation of the

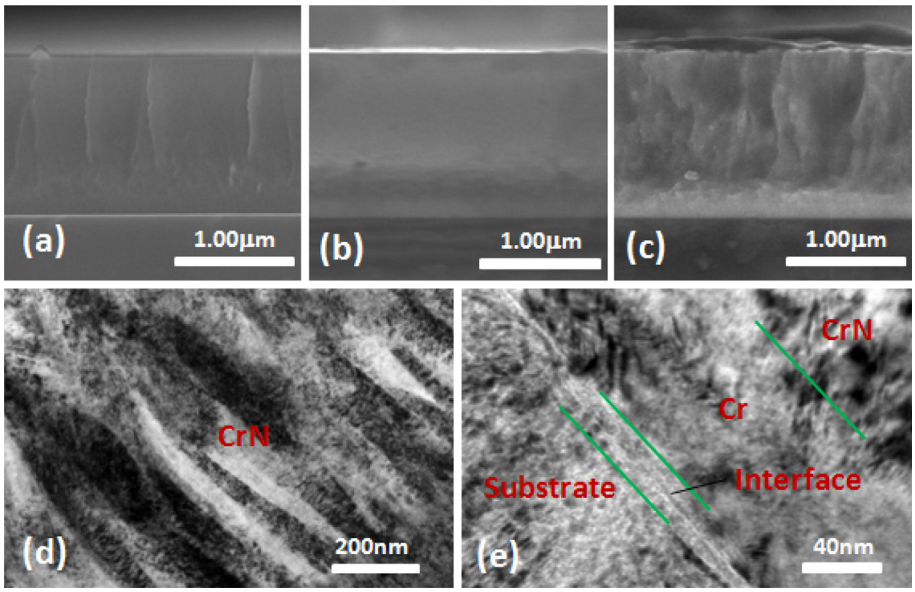

Fig. 1. Cross-sectional SEM morphology of the Cr–N coatings fabricated by (a) DCMS at −100 V DC bias, (b) HPPMS at −100 V DC bias and (c) HPPMS-PIII&D at −12 kV pulsed bias; (d) Cross-sectional TEM morphology of Cr–N columns in the HPPMS-PIII&D sample and (e) Interface between the Cr–N coating and substrate of the HPPMS-PIII&D sample.

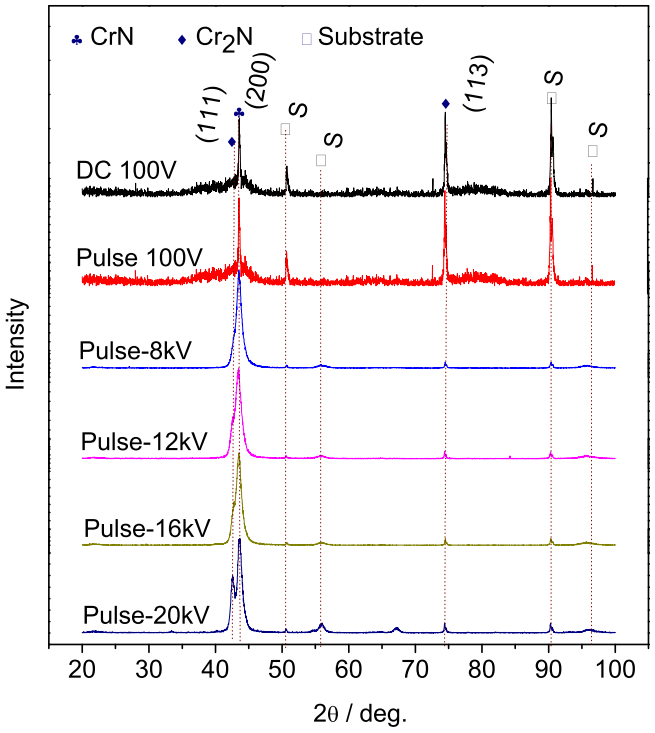

Fig. 2. XRD spectra of the as-prepared Cr–N coatings fabricated by DCMS and HPPMS at −100 V DC bias and HPPMS-PIII&D at pulsed biases of −8 kV, −12 kV, −16 kV, and −20 kV.

HPPMS sample is similar but a little weaker than that of the DCMS sample. With regard to the HPPMS-PIII&D samples (Fig. 3b), the intensity of the CrN(200) peak decreases with annealing temperature. Cr_2N(111) also appears and its intensity increases gradually becoming the dominant one after annealing at 800 °C. However, no obvious oxidation peaks can be observed thus indicating excellent oxidation resistance albeit the high temperature.

The trend of CrN being replaced by Cr_2N and Cr_2O_3 gradually can be observed from all the samples prepared by the different techniques as the annealing temperature goes up. The increase in the O and decrease of the N contents are consistent with those reported previously and mainly due to the low oxidation energy potential of Cr [17]. Formation of Cr_2N may be the consequence of incomplete denitrification or the reaction between denitrided Cr and N_2 in the air [18].

Generally, the oxidation temperature of CrN coatings is about 500 °C [10,11], as corroborated by our DCMS and HPPMS sample. In contrast, no obvious oxidation peaks can be found from the HPPMS-PIII&D samples, suggesting a much higher oxidation temperature of up to 800 °C. The high resistance can be attributed to energetic ion bombardment which improves the density of the CrN coatings, as shown in the Fig. 1c. Furthermore, the dense films inhibit diffusion of O resulting in excellent oxidation resistance up to 800 °C.

Fig. 4 shows the hardness and elastic module of the Cr–N films fabricated by DCMS and HPPMS at −100 V DC bias and HPPMS-PIII&D at −12 kV pulsed bias after annealing at different temperature up to 800 °C. Before annealing, all the samples have high hardness of about 25 Gpa and retain the high hardness up to 600 °C. The hardness of the DCMS and HPPMS samples drop sharply if the annealing temperature is higher than 600 °C, especially for the DCMS sample, dropping to 6.5 GPa after annealing at 800 °C. In comparison, the sample prepared by HPPMS-PIII&D shows much less decrease in the hardness which is 18 GPa even after annealing at 800 °C. The trend displayed by the elastic module is similar.

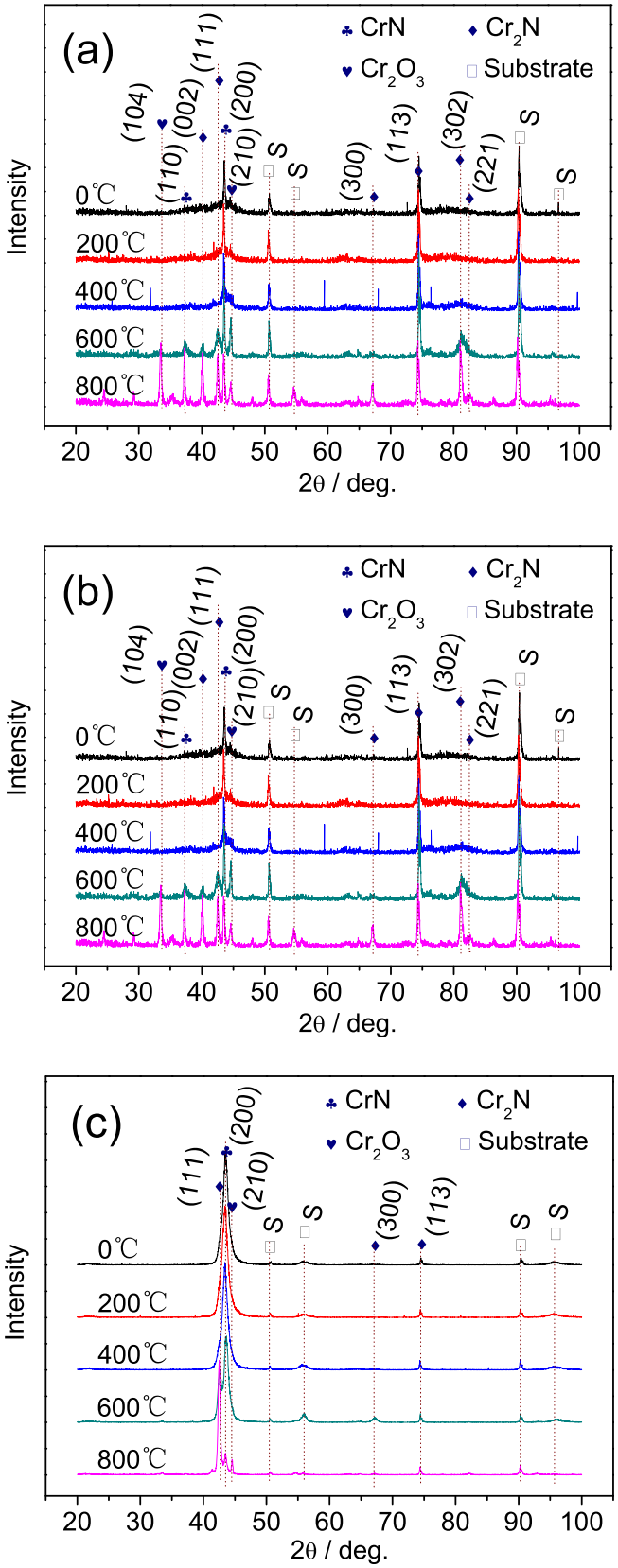

Fig. 3. XRD spectra of the Cr–N coatings fabricated by DCMS and HPPMS at −100 V DC bias and HPPMS-PIII&D at −12 kV pulsed bias after annealing at different temperature.

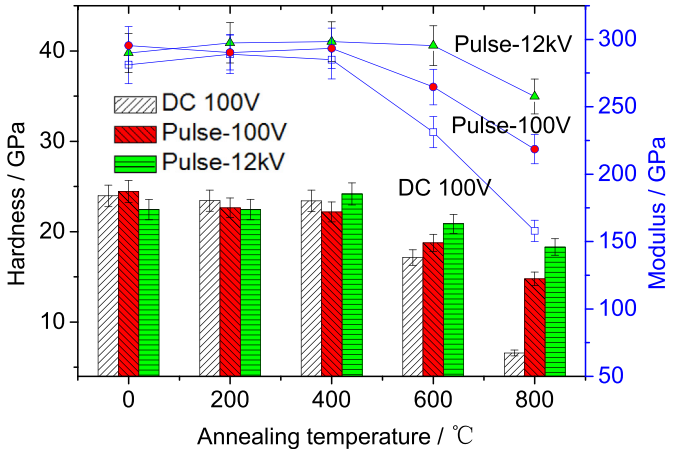

Fig. 4. Hardness (columns) and elastic modulus (lines) of Cr–N films fabricated by DCMS and HPPMS at −100 V DC bias and HPPMS-PIII&D at −12 kV pulsed bias after annealing at different temperature.

The hardness decrease observed from the DCMS and HPPMS sample is more significant than that of the HPPMS-PIII&D sample. The reasons for the different trends in the hardness versus annealing temperature are studied based on the XRD data. For the DCMS and HPPMS sample, the large drop in the hardness after annealing at 600 °C stems from oxidation but on the other hand, no obvious oxidation appears from the HPPMS-PIII&D samples, while the co-existence of CrN and Cr_2N formed during annealing may reduce the hardness [19].

Fig. 5 displays the polarization curves of Cr–N films fabricated by DCMS and HPPMS at −100 V DC bias and HPPMS-PIII&D at −12 kV pulsed bias after annealing. All samples exhibit a high corrosion potential before annealing. Higher corrosion potentials are observed from the HPPMS-PIII&D samples than the DCMS and HPPMS one, suggesting improved corrosion resistance. After annealing, the corrosion resistance of the three samples deteriorates. In particular, the corrosion potentials of the DCMS samples decrease sharply to about −0.6 V after annealing at 400 °C–800 °C (Fig. 5a). In comparison, the degradation observed from the HPPMS-PIII&D samples is less and the largest decrease is to −0.552 V which happens only in the sample after annealing at 600 °C. The polarization curves acquired from the samples after high temperature annealing are almost the same with that of the pristine sample prepared by HPPMS-PII&D at −12 kV.

The corrosion resistance of the coatings depends on the surface morphology and structure such as density and adhesion between coatings and substrates. Formation of channels for oxidation and corrosion is more difficult in a coating with a smooth surface, dense structure, and mixed interface [20]. As aforementioned, serious oxidation occurs in the loosely packaged columns and clean interface of the DCMS and HPPMS sample, giving rise to coating exfoliation and emergence of corrosion spots. Comparatively, the super dense structure formed HPPMS-PIII&D retards oxidation and corrosion channels cannot be readily formed in the films. Hence, at higher temperature tolerance is achieved from the HPPMS-PIII&D sample.

In conclusion, the densest Cr–N coatings are prepared by HPPMS-PIII&D at different bias voltages and high thermal oxidation resistance is observed at up to 800 °C compared to the normal oxidation temperature of about 500 °C reported in the literature. Both the hardness and thermal corrosion resistance of the HPPMS-PIII&D samples are improved significantly compared to the conventional DCMS and HPPMS sample. The excellent properties can be attributed to the dense structure, excellent adhesion, and phase

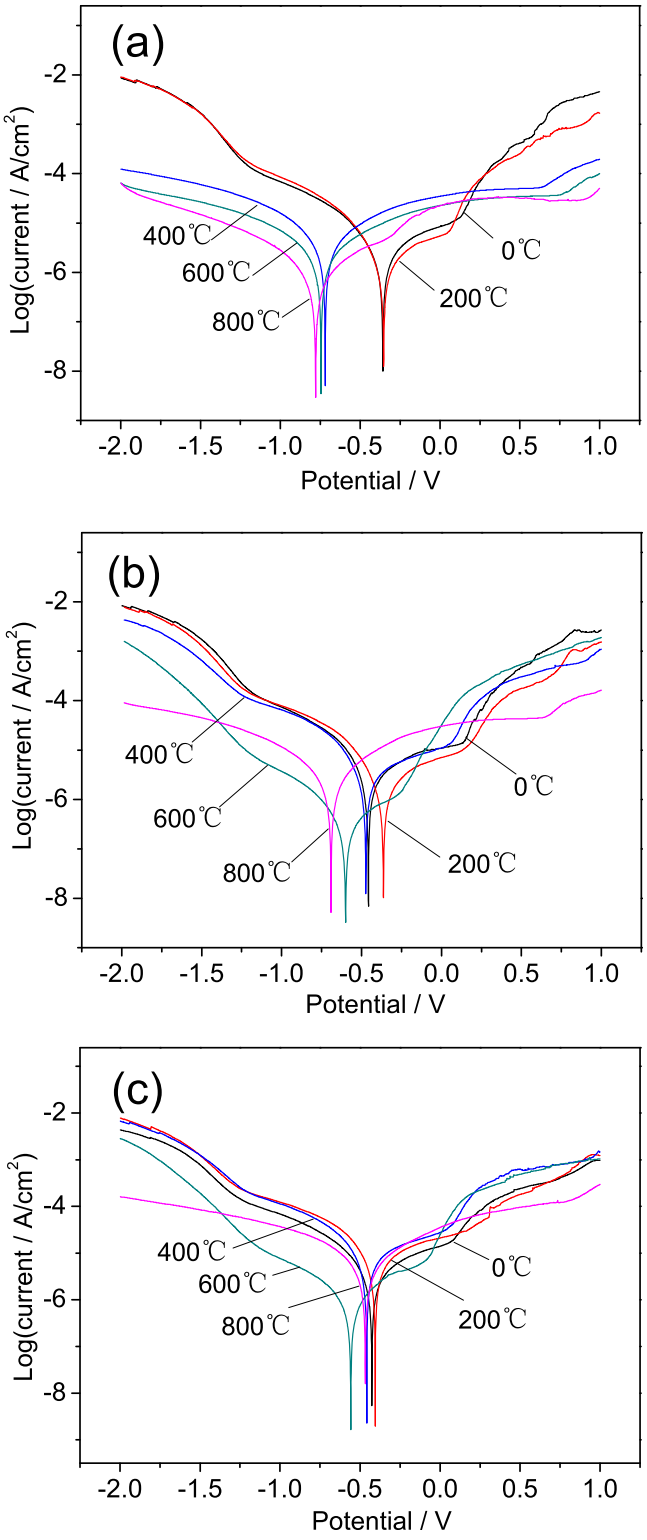

Fig. 5. Polarization curves of the Cr–N films fabricated by DCMS and HPPMS at −100 V DC bias and HPPMS-PIII&D at −12 kV pulsed bias after annealing at different temperature.

transition from CrN to the Cr_2N without obvious oxidation. Our results suggest that the combination of high ionization and high energy in HPPMS-PIID leads to the formation of super dense and adhesive Cr–N coatings which offer good oxidation and corrosion protection to up to 800 °C.

Acknowledgments

This work was financially supported jointly by National Natural Science Foundation of China (No. 51301004, U1330110), China Postdoctoral Science Foundation (No. 2013M530010), State Key Lab of Advanced Welding and Joining, Harbin Institute of Technology (No. AWJ-M13-13), and City University of Hong Kong Applied Research Grant (ARG) No. 9667066 and 9667069.

References

[1] Bobzin K, Bagcivan N, Immich P, Bolz S, Cremer R, Leyendecker T. Mechanical properties and oxidation behaviour of (Al,Cr)N and (Al,Cr,Si)N coatings for cutting tools deposited by HPPMS. Thin Solid Films 2008;517:1251–6.
[2] Kear BH, Thompson ER. Aircraft gas turbine materials and processes. Science 1980;208:847–910.
[3] Thanneeru R, Patil S, Deshpande S, Seal S. Effect of trivalent rare earth dopants in nanocrystalline ceria coatings for high-temperature oxidation resistance. Acta Mater 2007;55:3457–510.
[4] Lin JL, Zhang NY, Sproul WD, Moore JJ. A comparison of the oxidation behavior of CrN films deposited using continuous dc, pulsed dc and modulated pulsed power magnetron sputtering. Surf Coat Technol 2012;206:3283–8.
[5] Chang KL, Chung SC, Lai SH, Shih HC. The electrochemical behavior of thermally oxidized CrN coatings deposited on steel by cathodic arc plasma deposition. Appl Surf Sci 2004;236:406–10.
[6] Wu ZZ, Tian XB, Shi JW, Gong CZ, Yang SQ, Chu PK. Novel plasma immersion ion implantation and deposition hardware and technique based on high power pulsed magnetron discharge. Rev Sci Instrum 2011;69:033511–5.
[7] Tian XB, Wu ZZ, Gong CZ. High power pulsed magnetron discharge plasma ion implantation and deposition; 2010. CN201010213894.4: 06.
[8] Wu ZZ, Tian XB, Gong CZ, Yang SQ. Effect of bias modes on structures and composition of CrN films prepared by high power pulsed magnetron sputtering. Rare Metal Mater Eng 2013;42:405.
[9] Wu ZZ, Tian XB, Gong CZ, Yang SQ, Chu PK. Micrograph and structure of CrN films prepared by plasma immersion ion implantation and deposition using HPPMS plasma source. Surf Coat Technol 2013;229:210–7.
[10] Kacsich T, Lieb KP, Schaper A, Schulte O. Oxidation of thin chromium nitride films: kinetics and morphology. J Phys Condens Matter 1996;8:10703.
[11] Benien H, Maushart J, Meyer M, Suchentrunk R. D.C. magnetron sputtering of oxidation-resistant chromium and CrN films monitored by optical emission spectrometry. Mater Sci Eng A 1991;139:126.
[12] Greczynski G, Jensen J, Hultman L. CrN_x films prepared by DC magnetron sputtering and high-power pulsed magnetron sputtering: a comparative study. IEEE Trans Plasma Sci 2010;38:3046–111.
[13] Lin J, Sproul WD, Moore JJ, Lee S. High rate deposition of thick CrN and Cr_2N coatings using modulated pulse power (MPP) magnetron sputtering. Surf Coat Technol 2011;205:3226–9.
[14] Greczynski G, Jensen J, Böhlmark J, Hultman L. Microstructure control of CrN_x films during high power impulse magnetron sputtering. Surf Coat Technol 2010;205:118–213.
[15] Bilek MMM, McKenzie DR. A comprehensive model of stress generation and relief processes in thin films deposited with energetic ions. Surf Coat Technol 2006;200:4345–410.
[16] Chen HY, Lu FH. Oxidation behavior of chromium nitride films. Thin Solid Films 2006;515:2179–86.
[17] Lu FH, Chen HY, Hung CH. Degradation of CrN films at high temperature under controlled atmosphere. J Vac Sci Technol A 2003;21:671–5.
[18] Mayrhofer PH, Rovere F, Moser M, Strondl C, Tietema R. Thermally induced transitions of CrN thin films. Scr Mater 2007;57:249–54.
[19] Han ZH, Tian JW, Dai JW, Zhang HJ, Li GY. Preparation and mechanical properties of magnetron sputtered CrN_x thin films. J Funct Mater 2002;33:500–3.
[20] Liu C, Leyland A, Bi Q, Matthews A. Corrosion resistance of multi-layered plasma-assisted physical vapour deposition TiN and CrN coatings. Surf Coat Technol 2001;141:164–210.